

Multilevel correction type of adaptive finite element method for Hartree–Fock equation*

Fei Xu[†]

Abstract

This paper proposes an efficient algorithm for solving the Hartree–Fock equation combining a multilevel correction scheme with an adaptive refinement technique to improve computational efficiency. The algorithm integrates a multilevel correction framework with an optimized implementation strategy. Within this framework, a series of linearized boundary value problems are solved, and their approximate solutions are corrected by solving small-scale Hartree–Fock equations in low-dimensional correction spaces. The correction space comprises a coarse space and the solution to the linearized boundary value problem, enabling high accuracy while preserving low-dimensional characteristics. The proposed algorithm efficiently addresses the inherent computational complexity of the Hartree–Fock equation. Innovative correction strategies eliminate the need for direct computation of large-scale nonlinear eigenvalue systems and dense matrix operations. Furthermore, optimization techniques based on precomputations within the correction space render the total computational workload nearly independent of the number of self-consistent field iterations. This approach significantly accelerates the solution process of the Hartree–Fock equation, effectively mitigating the traditional exponential scaling demands on computational resources while maintaining precision.

Keywords. Hartree–Fock equation, adaptive finite element method, multilevel correction method.

AMS subject classifications. 65N30, 65H17, 35J10, 47J26.

1 Introduction

The Hartree–Fock equation [20, 55] plays an important role in quantum physics, condensed matter physics, and quantum chemistry. It is used to address multielectron systems, particularly in determining the electronic structure of atoms, molecules, and condensed matter. The physical significance of the equation lies in its approach to approximately calculating the ground-state energy and wavefunction of a multielectron system by iteratively solving for the electron wavefunction and electron density. At its core idea, the method represents the multielectron wavefunction as a Slater determinant of single-electron wavefunctions. With the rapid development of computer technology, the Hartree–Fock method has become widely used and extensively studied. Although the method has limitations, such as its inability to handle strongly correlated electron systems, it remains a fundamental tool for studying the electronic structures of multielectron systems. In particular, for simple atoms, molecules, and condensed matter, the Hartree–Fock method provides accurate results. It also serves as the foundation for most *ab initio* wavefunction-based methods used to solve the electronic Schrödinger equation. The method also shares considerable similarities with density functional theory (DFT) approaches [28], as the Kohn–Sham equations [33] differ only by the inclusion of an additional exchange-correlation potential. Under the local density approximation (LDA) [33] and the generalized gradient approximation (GGA) [48], Kohn–Sham equations avoid the computation of the exact exchange potential required in Hartree–Fock equations. However, many modern functionals are hybrids that include a portion of the exact exchange functional. Solving Kohn–Sham equations with hybrid functionals [8] requires a computational effort similar to that of solving the Hartree–Fock equation, in addition to the numerical integration of the exchange-correlation

*This work was supported by the Project of Cultivation for young top-motch Talents of Beijing Municipal Institutions (Grant No. BPHR202203022), the Beijing Municipal Natural Science Foundation (Grant No. 1232001), and the National Natural Science Foundation of China (Grant No. 12371386).

[†]School of Mathematics, Statistics and Mechanics, Beijing University of Technology, Beijing, 100124, P.R. China.
(fxu@bjut.edu.cn)

potential. Therefore, designing an efficient numerical algorithm for the Hartree–Fock equation is also foundational for solving hybrid DFT.

There are many challenges in solving the Hartree–Fock equation numerically. First, it is a complex nonlinear system that describes interactions among electrons in a multielectron system, including both exchange and Coulomb repulsion interactions. This complexity necessitates the use of iterative numerical methods to obtain approximate solutions. Second, as the number of electrons in the system increases, the dimensionality of the Hartree–Fock equation grows rapidly, resulting in a sharp increase in computational and storage demands. Solving the Hartree–Fock equation for large-scale systems becomes extremely time-consuming, often exceeding available computational resources. Therefore, reducing computational cost and storage requirements while maintaining solution accuracy remains a key challenge. Additionally, the numerical solution process is influenced by the stability and convergence of the algorithm. Hence, developing efficient numerical methods capable of accurately simulating large-scale systems continues to be a major challenge in computational quantum physics and chemistry.

After discretization, the exchange interaction in the Hartree–Fock equation leads to matrices with many nonzero elements (i.e., dense matrices). These require more data to be processed during computation, thereby reducing computational efficiency. In large-scale simulations, the multiplication and storage of dense matrices significantly increase computational costs. Consequently, most current methods for solving the Hartree–Fock equation rely on small basis set approaches, such as the local basis set method [17, 22, 23, 45, 51]. Meanwhile, the plane-wave method is also widely used [9, 16, 21, 31, 34, 41, 44, 53]. The finite element method (FEM) generally requires more degrees of freedom than the local basis set and plane-wave methods, rendering it extremely difficult to apply to the Hartree–Fock equation. However, FEM is particularly valuable when high-accuracy calculations are needed. By introducing more basis functions, FEM improves computational precision in describing the electronic structure of a system. Pask et al. [46] summarized the principles and advantages of FEM, noting its ability to provide solutions at predefined resolutions in real space using either periodic or nonperiodic wavefunctions. Nonperiodic functions are particularly useful for calculating the electronic properties of structures such as bent nanotubes or isolated molecules. However, FEM results in a significant increase in computational workload and resource demand, particularly for large-scale systems. Thus, applying FEM to the Hartree–Fock equation remains relatively difficult. Developing efficient numerical algorithms tailored for FEM is therefore both important and challenging.

Previous efforts have explored integrating FEM with the Hartree–Fock method. Flores et al. [18, 19] used higher-order polynomials as basis functions to solve two-dimensional atomic Hartree–Fock equations. Heinemann et al. [25] achieved high accuracy for light atoms and diatomic molecules using up to sixth-order Lagrange polynomials and prolate spheroidal coordinates, which significantly reduced computational cost but limited the range of applicable problems. In another study [26], spin polarization was examined using the Hartree–Fock–Slater method. Lavor et al. [35] proposed a global optimization approach using nonconvex polynomials as a variant of FEM. Sundholm et al. [57, 58] investigated finite-element multiconfiguration Hartree–Fock calculations for various atoms and compounds. Ackermann and Roitzsch [2, 3] applied a multigrid adaptive FEM in cylindrical coordinates for symmetric single-electron systems. Quiney et al. [49] compared finite basis set and FEM approaches for solving the relativistic Dirac equation. White et al. [60] used second-order orthonormal shape functions on a uniform mesh for one- and two-electron systems. Although two-dimensional FEM-based Hartree–Fock calculations have been widely studied, the three-dimensional case is more complex and less explored. In [4], a finite element Hartree–Fock method was introduced for polyatomic molecules using an accelerated exact exchange calculation with auxiliary local fitting. A divide-and-conquer method was also employed for parallelization and reduced computational scaling in complex systems. In [10], Braun introduced a three-dimensional FEM approach for solving closed-shell Hartree–Fock equations in small molecules, using a factorized Green’s function to solve both three-dimensional Schrödinger-type and Poisson equations. Additional results are available in [13, 24, 40, 43, 50, 52, 56] and the references cited therein. As the Hartree–Fock equation is studied across disciplines such as computational mathematics, physics, and chemistry, only a portion of the relevant literature can be cited here.

To improve the accuracy and efficiency of numerical simulations of the three-dimensional Hartree–Fock equation, we adopt the multilevel correction method described in [29, 30, 62], combined with an efficient implementation strategy. We also incorporate an adaptive refinement technique to address singularities [6, 14]. Using the multilevel correction method, we solve a set of linearized boundary value problems and refine their approximate solutions by solving small-scale Hartree–Fock equations in a low-dimensional cor-

rection space. This correction space comprises a coarse space and the solution to the linearized boundary value problem. This approach avoids solving the large-scale equation directly and significantly improves computational efficiency. In the correction space, we perform self-consistent field (SCF) iterations to solve the small-scale Hartree–Fock equation. To further enhance efficiency, we introduce two acceleration strategies. First, we construct separate correction spaces for each wavefunction independently. This ensures that the dimensionality of each correction space remains low and independent of the number of wavefunctions being solved. Moreover, the independent structure of these spaces facilitates parallel computation. Second, because the coarse space that forms part of the correction space remains fixed, the approximate wavefunctions that serve as basis functions for the correction space are retained after each adaptive refinement. A large portion of the computational workload can be preprocessed using tensor computation techniques. Subsequent iterations then require only simple matrix and tensor operations to complete the solution process. This strategy renders the computational cost of the algorithm independent of the number of SCF iterations. By employing multilevel correction techniques, we avoid large-scale nonlinear eigenvalue problems and dense matrix operations. Therefore, the multilevel correction algorithm significantly accelerates the solution of the Hartree–Fock equation.

The remainder of this paper is organized as follows: In Section 2, we review fundamental concepts and the finite element method for the Hartree–Fock equation. Section 3 discusses the construction of the corresponding multilevel correction type of adaptive finite element method. In Section 4, we present an efficient implementation of the correction step within the correction space. Section 5 introduces numerical experiments to demonstrate the effectiveness of the proposed method. Finally, Section 6 provides concluding remarks.

2 Finite element method for Hartree–Fock equation

In this study, we consider a molecular system comprising M nuclei with charges Z_1, \dots, Z_M and locations R_1, \dots, R_M with N electrons. The energy of the considered molecular system is described by:

$$\begin{aligned} E_{HF} = & \int_{\mathbb{R}^3} \left(\frac{1}{2} \sum_{\ell=1}^N |\nabla \phi_\ell|^2 - \sum_{k=1}^M \frac{Z_k}{|x - R_k|} \rho(x) \right) dx + \frac{1}{2} \int_{\mathbb{R}^3} \int_{\mathbb{R}^3} \frac{\rho(x)\rho(y)}{|x - y|} dx dy \\ & - \frac{1}{2} \int_{\mathbb{R}^3} \int_{\mathbb{R}^3} \frac{|P(x, y)|^2}{|x - y|} dx dy, \end{aligned} \quad (2.1)$$

where the density matrix $P(x, y) = \sum_{\ell=1}^N \phi_\ell(x)\phi_\ell^*(y)$, the density function $\rho(x) = P(x, x) = \sum_{\ell=1}^N |\phi_\ell(x)|^2$.

The corresponding Euler–Lagrange equation for the minimum Hartree–Fock energy is just the Hartree–Fock equation:

$$-\frac{1}{2} \Delta \phi_\ell + V_{\text{ext}} \phi_\ell + V_{\text{Har}}(\rho) \phi_\ell + V_{\text{x}}(P) \phi_\ell = \lambda_\ell \phi_\ell, \quad \ell = 1, \dots, N, \quad (2.2)$$

where the external potential V_{ext} , the Hartree potential $V_{\text{Har}}(\rho)$ and the exchange potential $V_{\text{x}}(P)$ are defined by:

$$V_{\text{ext}} = - \sum_{k=1}^M \frac{Z_k}{|x - R_k|}, \quad (2.3)$$

$$V_{\text{Har}}(\rho) = \int_{\mathbb{R}^3} \frac{\rho(y)}{|x - y|} dy, \quad (2.4)$$

$$V_{\text{x}}(P) \phi_\ell = - \int_{\mathbb{R}^3} \frac{P(x, y)}{|x - y|} \phi_\ell(y) dy. \quad (2.5)$$

As wavefunctions decay exponentially to zero, we assume that the numerical simulations are implemented in the bounded domain Ω . To apply the FEM, we provide a variational form of the Hartree–Fock equation (2.2) as follows:

$$\frac{1}{2} (\nabla \phi_\ell, \nabla \psi) + (V_{\text{ext}} \phi_\ell, \psi) + (V_{\text{Har}}(\rho) \phi_\ell, \psi) + (V_{\text{x}}(P) \phi_\ell, \psi) = (\lambda_\ell \phi_\ell, \psi), \quad \forall \psi \in H_0^1(\Omega), \quad (2.6)$$

where $(\phi, \psi) = \int_{\Omega} \phi \psi^* d\Omega$ denotes the standard L^2 -inner product.

Next, we generate a decomposition \mathcal{T}_h in computing domain Ω . Using mesh \mathcal{T}_h , we construct a finite element space V_h which is composed of piecewise polynomials. Then, the FEM is used to solve the following discrete Hartree–Fock equation:

$$\frac{1}{2}(\nabla \phi_{\ell,h}, \nabla \psi_h) + (V_{\text{ext}} \phi_{\ell,h}, \psi_h) + (V_{\text{Har}}(\rho_h) \phi_{\ell,h}, \psi_h) + (V_{\text{x}}(P_h) \phi_{\ell,h}, \psi_h) = (\lambda_{\ell,h} \phi_{\ell,h}, \psi_h), \quad \forall \psi_h \in V_h.$$

Because the discrete Hartree–Fock equation is a nonlinear eigenvalue problem, the SCF iteration should be adopted to derive the approximate solutions gradually. Hence, a linearized eigenvalue problem should be solved at each iteration step. The standard SCF iteration is presented in Algorithm 2.1 as follows:

Algorithm 2.1. *SCF Iteration for Hartree–Fock equation*

1. Given an initial value $\phi_{\ell,h}^{(1)}$, $\ell = 1, 2, \dots, N$, and a tolerance TOL .
2. Set $p = 1$.
3. Derive the new approximate wavefunctions $\phi_{\ell,h}^{(p+1)}$, $\ell = 1, 2, \dots, N$ by solving the following linearized eigenvalue problems:

$$\begin{aligned} & \frac{1}{2}(\nabla \phi_{\ell,h}^{(p+1)}, \nabla \psi_h) + (V_{\text{ext}} \phi_{\ell,h}^{(p+1)}, \psi_h) + (V_{\text{Har}}(\rho_h^{(p)}) \phi_{\ell,h}^{(p+1)}, \psi_h) + (V_{\text{x}}(P_h^{(p)}) \phi_{\ell,h}^{(p+1)}, \psi_h) \\ &= (\lambda_{\ell,h}^{(p+1)} \phi_{\ell,h}^{(p+1)}, \psi_h), \quad \forall \psi_h \in V_h. \end{aligned} \quad (2.7)$$

4. if $|E^{p+1} - E^p|/|E^{p+1}| \leq TOL$, stop. Else set $p = p + 1$ and go to Step 3.

For the Hartree potential $V_{\text{Har}}(\rho_h)$, we can derive an approximation by solving the following Poisson equation:

$$-\Delta V_{\text{Har}}(\rho_h) = 4\pi \rho_h(x). \quad (2.8)$$

Since the wavefunction of the Hartree–Fock equation decreases exponentially, zero Dirichlet boundary conditions can be adopted when the computational domain Ω is sufficiently large. However, since the solution of equation (2.8) decays linearly, simply using the zero Dirichlet boundary condition introduces a large truncation error at the boundary. In order to guarantee the accuracy, we approximate boundary values using multipole expansion [7].

For the exchange potential, based on the definition of density matrix, we obtain

$$\begin{aligned} (V_{\text{x}}(P) \psi_j, \psi_i) &= -\left(\int_{\Omega} \frac{\rho(x, y)}{|x - y|} \psi_j(y) dy, \psi_i(x)\right) \\ &= -\left(\int_{\Omega} \frac{\sum_{\ell=1}^N \phi_{\ell}(x) \phi_{\ell}^*(y)}{|x - y|} \psi_j(y) dy, \psi_i(x)\right) \\ &= -\sum_{\ell=1}^N \int_{\Omega} \left(\int_{\Omega} \frac{\phi_{\ell}^*(y) \psi_j(y)}{|x - y|} dy\right) \phi_{\ell}(x) \psi_i(x) dx. \end{aligned} \quad (2.9)$$

Thus, a dense matrix will be derived by discretizing the exchange potential. Meanwhile, to discretize (2.9), we need to first solve the functions $\int_{\Omega} \frac{\phi_{\ell}^*(y) \psi_j(y)}{|x - y|} dy$, which requires solving NN_h Poisson equations with $N_h = \dim(V_h)$. Thus, it is quite a time-consuming step to discretize the exchange potential.

3 Multilevel correction type of adaptive finite element method for Hartree–Fock equation

The numerical solution of the Hartree–Fock equation investigated in this study is extremely challenging. First, it is a nonlinear eigenvalue model that must be solved using SCF iterations and mixing schemes [32, 47]. Meanwhile, each iteration step involves solving a linear eigenvalue problem. As we know, it is quite

difficult to solve large-scale eigenvalue problems, and the computational workload increases exponentially. Next, owing to the presence of the exchange potential, the matrix obtained after discretizing the eigenvalue model becomes dense. This significantly increases the difficulty of addressing storage-related challenges. When the numerical algorithm involves a large amount of basis functions, such as with the FEM, numerical simulations become highly demanding. Thus, to date, there are very few finite element algorithms available for solving the Hartree–Fock equation in three-dimensional space.

In order to improve the efficiency and accuracy of the numerical simulation, we design a multilevel correction type of adaptive algorithm for solving the Hartree–Fock equation in this paper. We first introduce the multilevel correction technique to decompose the Hartree–Fock equation to reduce the computational difficulty. Subsequently, the adaptive refinement technique is combined to address the singularities, thereby forming a complete multilevel correction adaptive algorithm. The idea of our algorithm is to solve the linearized boundary value problem in the adaptive finite element space to get the approximate solution of the wavefunction. The exchange potential is placed on the righthand side of the linearized equation to reduce the computational complexity. Thus, this linearized boundary value problem requires significantly less computational effort compared with a full nonlinear eigenvalue problem. However, using a boundary value problem to approximate a nonlinear eigenvalue problem inevitably introduces errors. In order to further improve the accuracy, we construct a low-dimensional correction space, which consists of a low-dimensional finite element space and the approximate solution of the linearized boundary value problem. So this correction space is highly accurate while maintaining a low dimensionality. Then we solve a small-scale Hartree–Fock equation in this correction space to get the final approximate solution of the current adaptive finite element space. Therefore, the difficult parts of solving the Hartree–Fock equation are all confined to a low-dimensional and high-precision space.

For each wavefunction, we construct an individual correction space based on the corresponding solution of the linearized boundary value problem, and correct each wavefunction separately. This approach avoids high-dimensional inner product calculations that arise in global solution procedures and preserves the orthogonality of different wavefunctions. Additionally, treating each wavefunction with a separate correction process is well-suited for parallel computation.

The algorithm operates continuously on a multilevel mesh sequence until the prescribed tolerance is achieved. Assume that we have obtained an approximate solution $(\lambda_{\ell,h_k}, \phi_{\ell,h_k})$ in the space V_{h_k} . The detailed process in space $V_{h_{k+1}}$ to derive a new approximation $(\lambda_{\ell,h_{k+1}}, \phi_{\ell,h_{k+1}})$ is described as follows:

Algorithm 3.1. *One correction step for Hartree–Fock equation*

1. *Solve the following linearized boundary value problem:*

$$\begin{aligned} & \frac{1}{2}(\nabla \tilde{\phi}_{\ell,h_{k+1}}, \nabla \psi_{h_{k+1}}) + (V_{\text{ext}} \tilde{\phi}_{\ell,h_{k+1}}, \psi_{h_{k+1}}) + (V_{\text{Har}}(\rho_{h_k}) \tilde{\phi}_{\ell,h_{k+1}}, \psi_{h_{k+1}}) \\ &= (\lambda_{\ell,h_k} \phi_{\ell,h_k}, \psi_{h_{k+1}}) - (V_x(P_{h_k}) \phi_{\ell,h_k}, \psi_{h_{k+1}}), \quad \forall \psi_{h_{k+1}} \in V_{h_{k+1}}. \end{aligned} \quad (3.1)$$

2. *Define a correction space $V_{H,h_{k+1}} = V_H + \text{span}\{\tilde{\phi}_{\ell,h_{k+1}}\}$ and solve the following small-scale Hartree–Fock equation:*

$$\begin{aligned} & \frac{1}{2}(\nabla \phi_{\ell,h_{k+1}}, \nabla \psi_{H,h_{k+1}}) + (V_{\text{ext}} \phi_{\ell,h_{k+1}}, \psi_{H,h_{k+1}}) \\ &+ (V_{\text{Har}}(\rho_{h_{k+1}}) \phi_{\ell,h_{k+1}}, \psi_{H,h_{k+1}}) + (V_x(P_{h_{k+1}}) \phi_{\ell,h_{k+1}}, \psi_{H,h_{k+1}}) \\ &= (\lambda_{\ell,h_{k+1}} \phi_{\ell,h_{k+1}}, \psi_{H,h_{k+1}}), \quad \forall \psi_{h_{k+1}} \in V_{H,h_{k+1}}. \end{aligned} \quad (3.2)$$

For simplicity, we summarize the two steps above using the following expressions:

$$(\lambda_{\ell,h_{k+1}}, \phi_{\ell,h_{k+1}}) = HFCorrection(\lambda_{\ell,h_k}, \phi_{\ell,h_k}, V_H, V_{h_{k+1}}). \quad (3.3)$$

As mentioned, the novel algorithm is executed on a multilevel mesh sequence. Therefore, the mesh must be gradually refined to generate this sequence. Owing to the singularity of the Hartree–Fock equation, the adaptive finite element method (AFEM) is a competitive choice. Based on an *a posteriori* error estimator, AFEM selects mesh elements with large errors for further refinement. After generating the new mesh, we solve the Hartree–Fock equation and obtain a new approximate solution. We then begin another loop by computing the *a posteriori* error estimator and selecting mesh elements for additional refinement. This iterative process can be described as follows:

... Solve → Estimate → Mark → Refine ...

To obtain $\mathcal{T}_{h_{k+1}}$ from \mathcal{T}_{h_k} , we first solve the discrete equation on \mathcal{T}_{h_k} to derive an approximate solution, and then compute the *a posteriori* error estimator for each mesh element. Next, we mark the elements with the largest errors and refine them such that the new mesh $\mathcal{T}_{h_{k+1}}$ remains shape-regular and conforming.

In our simulation, the residual type *a posteriori* error estimation is employed to generate the error indicator. First, we construct the element residual $\mathcal{R}_T(\{\lambda_{\ell,h_k}, \phi_{\ell,h_k}\}_{\ell=1}^N)$ and the jump residual $\mathcal{J}_e(\{\phi_{\ell,h_k}\}_{\ell=1}^N)$ for the eigenpair approximation $(\lambda_{\ell,h_k}, \phi_{\ell,h_k})$, $\ell = 1, \dots, N$ as follows:

$$\mathcal{R}_T(\{\lambda_{\ell,h_k}, \phi_{\ell,h_k}\}_{\ell=1}^N) := \left(-\frac{1}{2} \Delta \phi_{\ell,h_k} + V_{\text{ext}} \phi_{\ell,h_k} + V_{\text{Har}}(\rho_{h_k}) \phi_{\ell,h_k} + V_{\text{x}}(P_{h_k}) \phi_{\ell,h_k} - \lambda_{\ell,h_k} \phi_{\ell,h_k} \right)_{\ell=1}^N, \quad \text{in } T \in \mathcal{T}_{h_k}, \quad (3.4)$$

$$\mathcal{J}_e(\{\phi_{\ell,h_k}\}_{\ell=1}^N) := \left(\frac{1}{2} \nabla \phi_{\ell,h_k} |_{T^+} \cdot \nu^+ + \frac{1}{2} \nabla \phi_{\ell,h_k} |_{T^-} \cdot \nu^- \right)_{\ell=1}^N, \quad \text{on } e \in \mathcal{E}_{h_k}, \quad (3.5)$$

where e is the common side of elements T^+ and T^- with the unit outward normals ν^+ and ν^- , \mathcal{E}_{h_k} denotes the set of interior faces of \mathcal{T}_{h_k} . For mesh element $T \in \mathcal{T}_{h_k}$, we define the local error indicator $\eta_{h_k}^2(\{\lambda_{\ell,h_k}, \phi_{\ell,h_k}\}_{\ell=1}^N, T)$ by

$$\eta_{h_k}^2(\{\lambda_{\ell,h_k}, \phi_{\ell,h_k}\}_{\ell=1}^N, T) := h_T^2 \|\mathcal{R}_T(\{\lambda_{\ell,h_k}, \phi_{\ell,h_k}\}_{\ell=1}^N)\|_{0,T}^2 + \sum_{e \in \mathcal{E}_{h_k}, e \subset \partial T} h_e \|\mathcal{J}_e(\{\phi_{\ell,h_k}\}_{\ell=1}^N)\|_{0,e}^2.$$

Given a subset $\widehat{\Omega} \subset \Omega$, we define the error estimate $\eta_{h_k}^2(\{\lambda_{\ell,h_k}, \phi_{\ell,h_k}\}_{\ell=1}^N, \widehat{\Omega})$ by

$$\eta_{h_k}^2(\{\lambda_{\ell,h_k}, \phi_{\ell,h_k}\}_{\ell=1}^N, \widehat{\Omega}) = \sum_{T \in \mathcal{T}_{h_k}, T \subset \widehat{\Omega}} \eta_{h_k}^2(\{\lambda_{\ell,h_k}, \phi_{\ell,h_k}\}_{\ell=1}^N, T). \quad (3.6)$$

Based on the error indicator (3.6), we use the Dörfler's marking strategy [15] described in Algorithm 3.2 to mark certain elements for local refinement.

Algorithm 3.2. *Dörfler's Marking Strategy*

1. Given a parameter $\theta \in (0, 1)$.
2. Construct a minimal subset \mathcal{M}_{h_k} from \mathcal{T}_{h_k} by selecting some elements in \mathcal{T}_{h_k} such that

$$\sum_{T \in \mathcal{M}_{h_k}} \eta_{h_k}^2(\{\lambda_{\ell,h_k}, \phi_{\ell,h_k}\}_{\ell=1}^N, T) \geq \theta \eta_{h_k}^2(\{\lambda_{\ell,h_k}, \phi_{\ell,h_k}\}_{\ell=1}^N, \Omega).$$

3. Mark all the elements in \mathcal{M}_{h_k} .

Based on the adaptive refinement scheme described above, and the one level correction step defined by Algorithm 3.1, the multilevel correction type of AFEM for Hartree–Fock equation is given below:

Algorithm 3.3. *Multilevel correction type of AFEM for Hartree–Fock equation*

1. Generate a coarse mesh \mathcal{T}_H on Ω and construct the corresponding coarse space V_H . Start with an initial mesh \mathcal{T}_{h_1} obtained by refining \mathcal{T}_H several times. Subsequently, establish the initial space V_{h_1} on \mathcal{T}_{h_1} and solve the Hartree–Fock equation:

$$\begin{aligned} & \frac{1}{2} (\nabla \phi_{\ell,h_1}, \nabla \psi_{h_1}) + (V_{\text{ext}} \phi_{\ell,h_1}, \psi_{h_1}) + (V_{\text{Har}}(\rho_{h_1}) \phi_{\ell,h_1}, \psi_{h_1}) + (V_{\text{x}}(P_{h_1}) \phi_{\ell,h_1}, \psi_{h_1}) \\ &= (\lambda_{\ell,h_1} \phi_{\ell,h_1}, \psi_{h_1}), \quad \ell = 1, \dots, N, \quad \forall \psi_{h_1} \in V_{h_1}. \end{aligned} \quad (3.7)$$

2. Set $k = 1$.
3. Compute the local error indicator $\eta_{h_k}(\{\lambda_{\ell,h_k}, \phi_{\ell,h_k}\}_{\ell=1}^N, T)$ for each mesh element $T \in \mathcal{T}_{h_k}$.
4. Construct $\mathcal{M}_{h_k} \subset \mathcal{T}_{h_k}$ by Dörfler's marking strategy and then refine \mathcal{T}_{h_k} to get a new mesh $\mathcal{T}_{h_{k+1}}$.
5. For $\ell = 1, \dots, N$, perform the following correction step to obtain $(\lambda_{\ell,h_{k+1}}, \phi_{\ell,h_{k+1}})$:

$$(\lambda_{\ell,h_{k+1}}, \phi_{\ell,h_{k+1}}) = \text{HFCorrection}(\lambda_{\ell,h_k}, \phi_{\ell,h_k}, V_H, V_{h_{k+1}}). \quad (3.8)$$

6. Let $k = k + 1$ and go to Step 3.

4 Efficient implementation of correction step

This section introduces the efficient strategy to implement the multilevel correction type of AFEM defined in the previous section. In each adaptive finite element space, we only need to solve some linearized boundary value problems without nonlinear iteration. Additionally, to avoid generating dense matrices, the exchange potential is placed on the righthand side of the equation. Thus, the computation time and storage space are significantly smaller compared to those required for solving the large-scale Hartree–Fock equation.

For the correction step defined in V_{H,h_k} , the SCF iteration is adopted to solve the small-scale Hartree–Fock equation. Then in each iteration step, we need to solve a small-scale linear dense eigenvalue problem. Because the dimension of the correction space ($N_H + 1$) is small compared to that of the adaptive finite element space (N_{h_k}), thus the computational efficiency and storage requirement are significantly improved relative to those of the large-scale dense eigenvalue problem. In the correction space, the solution of the linearized boundary value problem is added as a basis function, thus the integral calculations associated with this basis function should be performed on the adaptive mesh to maintain the accuracy. Additionally, complex molecular systems often require numerous SCF iterations, with each iteration repeating the solution process. Hence, for the multilevel correction type of AFEM, the most time-consuming step is the correction process defined in the low-dimensional correction space if we adopt the traditional SCF scheme described in Algorithm 2.1.

To improve the efficiency of solving the small-scale Hartree–Fock equation, we next present an efficient strategy for implementing the correction step. As the coarse space V_H remains unchanged throughout the algorithm and the newly added basis function remains fixed during the SCF iteration, we can perform the invariant computations outside the SCF iteration. Hence, each iteration step requires only a few simple matrix operations. In addition, most steps in the computation process support parallelization. For example, the linearized boundary problems and correction spaces are all constructed separately for each wavefunction.

Next, we will use the ℓ -th wavefunction as an example to illustrate the implementation process of the correction step, which is the same for all the other wavefunctions. For the description of implementing technique here, let $\{\psi_{j,H}\}_{1 \leq j \leq N_H}$ denote the Lagrange basis function for the coarse finite element space V_H , and $\tilde{\phi}_{\ell,h}$ denote the added basis function in the correction space $V_{H,h}$. Then the correction space for the ℓ -th wavefunction can be described by $V_{H,h} = \{\tilde{\phi}_{\ell,h}, \psi_{1,H}, \dots, \psi_{N_H,H}\}$.

In order to show the main idea here, we consider the matrix version of eigenvalue problem (3.2). Since a new basis function is added, the corresponding matrix should have one more row and one more column. The detailed form can be described as follows:

$$\begin{pmatrix} A_H & b_{Hh} \\ b_{Hh}^T & \beta \end{pmatrix} \begin{pmatrix} C_H \\ \theta \end{pmatrix} = \lambda_{\ell,h} \begin{pmatrix} M_H & c_{Hh} \\ c_{Hh}^T & \gamma \end{pmatrix} \begin{pmatrix} C_H \\ \theta \end{pmatrix}, \quad (4.1)$$

where $\dim(A_H) = \dim(M_H) = N_H \times N_H$, $\dim(b_{Hh}) = \dim(c_{Hh}) = N_H \times 1$, $\dim(C_H) = N_H \times 1$ and $\dim(\beta) = \dim(\gamma) = \dim(\theta) = 1$.

Based on the Hartree–Fock equation (3.2), the matrix M_H has the following form:

$$(M_H)_{i,j} = \int_{\Omega} \psi_{j,H} \psi_{i,H} dx, \quad (c_{Hh})_i = \int_{\Omega} \tilde{\phi}_{\ell,h} \psi_{i,H} dx, \quad \gamma = \int_{\Omega} |\tilde{\phi}_{\ell,h}|^2 dx. \quad (4.2)$$

It is obvious that the matrix M_H will not change throughout the algorithm. The vector c_{Hh} and the scalar γ rely on the basis function $\tilde{\phi}_{\ell,h}$. As the basis function $\tilde{\phi}_{\ell,h}$ remains unchanged in the correction space, thus the vector c_{Hh} and the scalar γ will not change during the SCF iteration in the correction space.

Because the wavefunction will be renewed at each iteration step, the stiffness matrix A_H , the vector b_{Hh} and the scalar β will change during the SCF iteration process. Then it is required to consider the efficient implementation to update the matrix A_H , the vector b_{Hh} and the scalar β .

Assume we have a given initial wavefunction $\phi_{\ell,Hh} \in V_{H,h}$ for the SCF iteration involved in the correction space. The approximate wavefunction $\phi_{\ell,Hh}$ can be expressed as $\phi_{\ell,Hh} = \tilde{\theta} \tilde{\phi}_{\ell,h} + \sum_{m=1}^{N_H} c_{m,H} \psi_{m,H}$. As $\phi_{\ell,Hh}$ is the given initial value, the coefficients $c_{1,H}, \dots, c_{m,H}, \tilde{\theta}$ are known, which is just the solution of (4.1) in the previous iteration step. In the subsequent iterative solving process, we will continually

update the value of $\phi_{\ell,Hh}$ (i.e., update the coefficients $c_{1,H}, \dots, c_{m,H}, \tilde{\theta}$). When we correct the ℓ -the wavefunction $\phi_{\ell,Hh}$ in its own correction space, the other wavefunctions are fixed as $\tilde{\phi}_{s,h}$ (i.e. $\phi_{s,Hh} = \tilde{\phi}_{s,h}$ if $s \neq \ell$) during the computation of the density function and density matrix.

From the definitions of the correction space $V_{H,h}$ and the eigenvalue problem (4.1), the matrix A_H has the following expansion:

$$\begin{aligned}
& (A_H)_{i,j} \\
&= \frac{1}{2} \int_{\Omega} \nabla \psi_{j,H}(x) \nabla \psi_{i,H}(x) dx + \int_{\Omega} V_{\text{ext}} \psi_{j,H}(x) \psi_{i,H}(x) dx \\
&\quad + \int_{\Omega} V_{\text{Har}}(\rho_{Hh}) \psi_{j,H}(x) \psi_{i,H}(x) dx + \int_{\Omega} (V_{\text{x}}(P_{Hh}) \psi_{j,H}) \psi_{i,H}(x) dx \\
&= \frac{1}{2} \int_{\Omega} \nabla \psi_{j,H}(x) \nabla \psi_{i,H}(x) dx + \int_{\Omega} V_{\text{ext}} \psi_{j,H}(x) \psi_{i,H}(x) dx \\
&\quad + \sum_{s=1}^N \int_{\Omega} \int_{\Omega} \frac{\phi_{s,Hh}(y) \phi_{s,Hh}^*(y)}{|x-y|} dy \psi_{j,H}(x) \psi_{i,H}(x) dx \\
&\quad + \sum_{s=1}^N \int_{\Omega} \int_{\Omega} \frac{\phi_{s,Hh}^*(y) \psi_{j,H}(y)}{|x-y|} dy \phi_{s,Hh}(x) \psi_{i,H}(x) dx. \tag{4.3}
\end{aligned}$$

Let us denote

$$(A_{\text{Kin}})_{i,j} = \frac{1}{2} \int_{\Omega} \nabla \psi_{j,H}(x) \nabla \psi_{i,H}(x) dx + \int_{\Omega} V_{\text{ext}} \psi_{j,H}(x) \psi_{i,H}(x) dx, \tag{4.4}$$

$$(A_{\text{Har},s})_{i,j} = \int_{\Omega} \int_{\Omega} \frac{\phi_{s,Hh}(y) \phi_{s,Hh}^*(y)}{|x-y|} dy \psi_{j,H}(x) \psi_{i,H}(x) dx, \tag{4.5}$$

$$(A_{\text{x},s})_{i,j} = \int_{\Omega} \int_{\Omega} \frac{\phi_{s,Hh}^*(y) \psi_{j,H}(y)}{|x-y|} dy \phi_{s,Hh}(x) \psi_{i,H}(x) dx. \tag{4.6}$$

The matrix A_{Kin} remains unchanged throughout the algorithm. Thus, we only need to calculate A_{Kin} one time at the beginning of the algorithm. When $s \neq \ell$, we have

$$\begin{aligned}
& (A_{\text{Har},s})_{i,j} + (A_{\text{x},s})_{i,j} \\
&= \int_{\Omega} \int_{\Omega} \frac{|\tilde{\phi}_{s,h}(y)|^2}{|x-y|} dy \psi_{j,H}(x) \psi_{i,H}(x) dx \\
&\quad + \int_{\Omega} \int_{\Omega} \frac{\tilde{\phi}_{s,h}^*(y) \psi_{j,H}(y)}{|x-y|} dy \tilde{\phi}_{s,h}(x) \psi_{i,H}(x) dx. \tag{4.7}
\end{aligned}$$

When $s = \ell$, we have

$$\begin{aligned}
& (A_{\text{Har},\ell})_{i,j} + (A_{\text{x},\ell})_{i,j} \\
&= \int_{\Omega} \int_{\Omega} \frac{\left| \tilde{\theta} \tilde{\phi}_{\ell,h}(y) + \sum_{m=1}^{N_H} c_{m,H} \psi_{m,H}(y) \right|^2}{|x-y|} dy \psi_{j,H}(x) \psi_{i,H}(x) dx \\
&\quad + \int_{\Omega} \left\{ \int_{\Omega} \frac{\left(\tilde{\theta} \tilde{\phi}_{\ell,h}(y) + \sum_{m=1}^{N_H} c_{m,H} \psi_{m,H}(y) \right)^* \psi_{j,H}(y)}{|x-y|} dy \right. \\
&\quad \left. \left(\tilde{\theta} \tilde{\phi}_{\ell,h}(x) + \sum_{m=1}^{N_H} c_{m,H} \psi_{m,H}(x) \right) \psi_{i,H}(x) \right\} dx. \tag{4.8}
\end{aligned}$$

For simplicity, let us denote

$$\begin{aligned}
\tilde{V}_{s,\ell}(x) &= \int_{\Omega} \frac{\tilde{\phi}_{s,h}(y) \tilde{\phi}_{\ell,h}^*(y)}{|x-y|} dy, \\
\tilde{V}_{s,m}(x) &= \int_{\Omega} \frac{\tilde{\phi}_{s,h}(y) \psi_{m,H}(y)}{|x-y|} dy,
\end{aligned}$$

$$V_{m,n}(x) = \int_{\Omega} \frac{\psi_{m,H}(y)\psi_{n,H}(y)}{|x-y|} dy.$$

Then (4.7) and (4.8) can be rewritten as

$$\begin{aligned} & (A_{\text{Har},s})_{i,j} + (A_{x,s})_{i,j} \\ &= \int_{\Omega} \tilde{\tilde{V}}_{s,s}(x)\psi_{j,H}(x)\psi_{i,H}(x)dx + \int_{\Omega} \tilde{V}_{s,j}^*(x)\tilde{\phi}_{s,h}(x)\psi_{i,H}(x)dx \end{aligned} \quad (4.9)$$

and

$$\begin{aligned} & (A_{\text{Har},\ell})_{i,j} + (A_{x,\ell})_{i,j} \\ &= \int_{\Omega} \left\{ \left(|\tilde{\theta}|^2 \tilde{\tilde{V}}_{\ell,\ell}(x) + \tilde{\theta} \sum_{m=1}^{N_H} c_{m,H}^* \tilde{V}_{\ell,m}(x) + \tilde{\theta}^* \sum_{m=1}^{N_H} c_{m,H} \tilde{V}_{\ell,m}^*(x) + \sum_{m,n=1}^{N_H} c_{m,H} c_{n,H}^* V_{m,n}(x) \right) \right. \\ & \quad \left. \psi_{j,H}(x)\psi_{i,H}(x) \right\} dx \\ & \quad + \int_{\Omega} \left(\tilde{\theta}^* \tilde{V}_{\ell,j}^*(x) + \sum_{m=1}^{N_H} c_{m,H}^* V_{j,m}(x) \right) \left(\tilde{\theta} \tilde{\phi}_{\ell,h}(x) + \sum_{m=1}^{N_H} c_{m,H} \psi_{m,H}(x) \right) \psi_{i,H}(x) dx. \end{aligned} \quad (4.10)$$

To further simplify the expression, we define

$$V_{m,n,j,i} = \int_{\Omega} V_{m,n}(x)\psi_{j,H}(x)\psi_{i,H}(x)dx, \quad (4.11)$$

$$\tilde{V}_{\ell,m,j,i} = \int_{\Omega} \tilde{V}_{\ell,m}(x)\psi_{j,H}(x)\psi_{i,H}(x)dx, \quad (4.12)$$

$$\tilde{\tilde{V}}_{\ell,j,i} = \int_{\Omega} \tilde{\tilde{V}}_{\ell,\ell}(x)\psi_{j,H}(x)\psi_{i,H}(x)dx, \quad (4.13)$$

$$\tilde{W}_{\ell,j,i} = \int_{\Omega} \tilde{V}_{\ell,j}(x)\tilde{\phi}_{\ell,h}(x)\psi_{i,H}(x)dx, \quad (4.14)$$

$$\tilde{W}_{*,\ell,j,i} = \int_{\Omega} \tilde{V}_{\ell,j}^*(x)\tilde{\phi}_{\ell,h}(x)\psi_{i,H}(x)dx. \quad (4.15)$$

Based on the definition of $\tilde{V}_{\ell,m,j,i}$, we can also derive $\tilde{V}_{\ell,i,j,m} = \int_{\Omega} V_{j,m}(x)\tilde{\phi}_{\ell,h}(x)\psi_{i,H}(x)dx$.

As we can see, $V_{m,n,j,i}$ remains unchanged during the whole algorithm. Thus, we can calculate $V_{m,n,j,i}$ at the beginning of the algorithm. Because $\tilde{\phi}_{\ell,h}$ remains unchange in each correction step, so $\tilde{V}_{\ell,m,j,i}$, $\tilde{\tilde{V}}_{\ell,j,i}$, $\tilde{W}_{\ell,j,i}$ and $\tilde{W}_{*,\ell,j,i}$ can be calculated before each correction step.

After calculating these quantities in advance, we can assemble $A_{\text{Har},\ell}$ and $A_{x,\ell}$ by:

$$(A_{\text{Har},s})_{i,j} + (A_{x,s})_{i,j} = \tilde{\tilde{V}}_{s,j,i} + \tilde{W}_{*,s,j,i} \quad (4.16)$$

and

$$\begin{aligned} & (A_{\text{Har},\ell})_{i,j} + (A_{x,\ell})_{i,j} \\ &= |\tilde{\theta}|^2 \tilde{\tilde{V}}_{\ell,j,i} + \tilde{\theta} \sum_{m=1}^{N_H} c_{m,H}^* \tilde{V}_{\ell,m,j,i} + \tilde{\theta}^* \sum_{m=1}^{N_H} c_{m,H} \tilde{V}_{\ell,m,j,i}^* + \sum_{m,n=1}^{N_H} c_{m,H} c_{n,H}^* V_{m,n,j,i} \\ & \quad + |\tilde{\theta}|^2 \tilde{W}_{*,\ell,j,i} + \tilde{\theta}^* \sum_{m=1}^{N_H} c_{m,H} \tilde{V}_{\ell,j,m,i}^* + \tilde{\theta} \sum_{m=1}^{N_H} c_{m,H}^* \tilde{V}_{\ell,i,j,m} + \sum_{m,n=1}^{N_H} c_{m,H}^* c_{n,H} V_{j,m,n,i}. \end{aligned} \quad (4.17)$$

Next, we begin to assemble the vector b_{Hh} . The vector b_{Hh} has the following expansion

$$(b_{Hh})_i = \frac{1}{2} \int_{\Omega} \nabla \tilde{\phi}_{\ell,h}(x) \nabla \psi_{i,H}(x) dx + \int_{\Omega} V_{\text{ext}} \tilde{\phi}_{\ell,h}(x) \psi_{i,H}(x) dx$$

$$\begin{aligned}
& + \int_{\Omega} V_{\text{Har}}(\rho_{Hh}) \tilde{\phi}_{\ell,h}(x) \psi_{i,H}(x) dx + \int_{\Omega} (V_{\text{x}}(P_{Hh}) \tilde{\phi}_{\ell,h}) \psi_{i,H}(x) dx \\
= & \frac{1}{2} \int_{\Omega} \nabla \tilde{\phi}_{\ell,h}(x) \nabla \psi_{i,H}(x) dx + \int_{\Omega} V_{\text{ext}} \tilde{\phi}_{\ell,h}(x) \psi_{i,H}(x) dx \\
& + \sum_{s=1}^N \int_{\Omega} \int_{\Omega} \frac{|\phi_{s,Hh}(y)|^2}{|x-y|} dy \tilde{\phi}_{\ell,h}(x) \psi_{i,H}(x) dx \\
& + \sum_{s=1}^N \int_{\Omega} \int_{\Omega} \frac{\phi_{s,Hh}^*(y) \tilde{\phi}_{\ell,h}(y)}{|x-y|} dy \phi_{s,Hh}(x) \psi_{i,H}(x) dx. \tag{4.18}
\end{aligned}$$

Denote

$$(b_{\text{Kin},\ell})_i = \frac{1}{2} \int_{\Omega} \nabla \tilde{\phi}_{\ell,h}(x) \nabla \psi_{i,H}(x) dx + \int_{\Omega} V_{\text{ext}} \tilde{\phi}_{\ell,h}(x) \psi_{i,H}(x) dx, \tag{4.19}$$

$$(b_{\text{Har},s,\ell})_i = \int_{\Omega} \int_{\Omega} \frac{|\phi_{s,Hh}(y)|^2}{|x-y|} dy \tilde{\phi}_{\ell,h}(x) \psi_{i,H}(x) dx, \tag{4.20}$$

$$(b_{\text{x},s,\ell})_i = \int_{\Omega} \int_{\Omega} \frac{\phi_{s,Hh}^*(y) \tilde{\phi}_{\ell,h}(y)}{|x-y|} dy \phi_{s,Hh}(x) \psi_{i,H}(x) dx. \tag{4.21}$$

It is obvious that $b_{\text{Kin},\ell}$ remains unchanged during the correction step. For $b_{\text{Har},s,\ell}$ and $b_{\text{x},s,\ell}$, when $s \neq \ell$, we have

$$\begin{aligned}
& (b_{\text{Har},s,\ell})_i + (b_{\text{x},s,\ell})_i \\
= & \int_{\Omega} \int_{\Omega} \frac{|\tilde{\phi}_{s,h}(y)|^2}{|x-y|} dy \tilde{\phi}_{\ell,h}(x) \psi_{i,H}(x) dx + \int_{\Omega} \left\{ \int_{\Omega} \frac{\tilde{\phi}_{s,h}^*(y) \tilde{\phi}_{\ell,h}(y)}{|x-y|} dy \tilde{\phi}_{s,h}(x) \psi_{i,H}(x) \right\} dx \\
= & \int_{\Omega} \tilde{\tilde{V}}_{s,s}(x) \tilde{\phi}_{\ell,h}(x) \psi_{i,H}(x) dx + \int_{\Omega} \tilde{\tilde{V}}_{\ell,s}(x) \tilde{\phi}_{s,h}(x) \psi_{i,H}(x) dx. \tag{4.22}
\end{aligned}$$

When $s = \ell$, we have

$$\begin{aligned}
& (b_{\text{Har},\ell,\ell})_i + (b_{\text{x},\ell,\ell})_i \\
= & \int_{\Omega} \int_{\Omega} \frac{\left| \tilde{\theta} \tilde{\phi}_{\ell,h}(y) + \sum_{m=1}^{N_H} c_{m,H} \psi_{m,H}(y) \right|^2}{|x-y|} dy \tilde{\phi}_{\ell,h}(x) \psi_{i,H}(x) dx \\
& + \int_{\Omega} \left\{ \int_{\Omega} \frac{\left(\tilde{\theta} \tilde{\phi}_{\ell,h}(y) + \sum_{m=1}^{N_H} c_{m,H} \psi_{m,H}(y) \right)^* \tilde{\phi}_{\ell,h}(y)}{|x-y|} dy \right. \\
& \quad \left. \left(\tilde{\theta} \tilde{\phi}_{\ell,h}(x) + \sum_{m=1}^{N_H} c_{m,H} \psi_{m,H}(x) \right) \psi_{i,H}(x) \right\} dx \\
= & \int_{\Omega} \left\{ \left(|\tilde{\theta}|^2 \tilde{\tilde{V}}_{\ell,\ell}(x) + \tilde{\theta} \sum_{m=1}^{N_H} c_{m,H}^* \tilde{V}_{\ell,m}(x) + \tilde{\theta}^* \sum_{m=1}^{N_H} c_{m,H} \tilde{V}_{\ell,m}^*(x) + \sum_{m,n=1}^{N_H} c_{m,H} c_{n,H}^* V_{m,n}(x) \right) \right. \\
& \quad \left. \tilde{\phi}_{\ell,h}(x) \psi_{i,H}(x) \right\} dx \\
& + \int_{\Omega} \left(\tilde{\theta}^* \tilde{\tilde{V}}_{\ell,\ell}(x) + \sum_{m=1}^{N_H} c_{m,H}^* \tilde{V}_{\ell,m}(x) \right) \left(\tilde{\theta} \tilde{\phi}_{\ell,h}(x) + \sum_{m=1}^{N_H} c_{m,H} \psi_{m,H}(x) \right) \psi_{i,H}(x) dx. \tag{4.23}
\end{aligned}$$

Define

$$\tilde{\tilde{V}}_{s,m,\ell,i} = \int_{\Omega} \tilde{\tilde{V}}_{s,m}(x) \tilde{\phi}_{\ell,h}(x) \psi_{i,H}(x) dx. \tag{4.24}$$

It is obvious that $\tilde{\tilde{V}}_{s,m,\ell,i}$ remains unchanged during the correction step. Then $b_{\text{Har},\ell}$ and $b_{\text{x},\ell}$ can be assembled in the following way:

$$(b_{\text{Har},s,\ell})_i + (b_{\text{x},s,\ell})_i = \tilde{\tilde{V}}_{s,s,\ell,i} + \tilde{\tilde{V}}_{\ell,s,s,i} \tag{4.25}$$

and

$$\begin{aligned}
& (b_{\text{Har},\ell,\ell})_i + (b_{\text{x},\ell,\ell})_i \\
= & |\tilde{\theta}|^2 \tilde{\tilde{V}}_{\ell,\ell,\ell,i} + \tilde{\theta} \sum_{m=1}^{N_H} c_{m,H}^* \tilde{W}_{\ell,m,i} + \tilde{\theta}^* \sum_{m=1}^{N_H} c_{m,H} \tilde{W}_{*,\ell,m,i} + \sum_{m,n=1}^{N_H} c_{m,H} c_{n,H}^* \tilde{V}_{\ell,i,m,n} \\
& + |\tilde{\theta}|^2 \tilde{\tilde{V}}_{\ell,\ell,\ell,i} + \tilde{\theta}^* \sum_{m=1}^{N_H} c_{m,H} \tilde{\tilde{V}}_{\ell,m,i} + \tilde{\theta} \sum_{m=1}^{N_H} c_{m,H}^* \tilde{W}_{\ell,m,i} + \sum_{m,n} c_{m,H}^* c_{n,H} \tilde{V}_{\ell,m,n,i}.
\end{aligned} \tag{4.26}$$

Finally, we come to assemble the scalar β . The scalar β has the following expansion

$$\begin{aligned}
\beta = & \frac{1}{2} \int_{\Omega} \nabla \tilde{\phi}_{\ell,h}(x) \nabla \tilde{\phi}_{\ell,h}^*(x) dx + \int_{\Omega} V_{\text{ext}} \tilde{\phi}_{\ell,h}(x) \tilde{\phi}_{\ell,h}^*(x) dx \\
& + \int_{\Omega} V_{\text{Har}}(\rho_{Hh}) \tilde{\phi}_{\ell,h}(x) \tilde{\phi}_{\ell,h}^*(x) dx + \int_{\Omega} (V_{\text{x}}(P_{Hh}) \tilde{\phi}_{\ell,h}) \tilde{\phi}_{\ell,h}^*(x) dx \\
= & \frac{1}{2} \int_{\Omega} \nabla \tilde{\phi}_{\ell,h}(x) \nabla \tilde{\phi}_{\ell,h}^*(x) dx + \int_{\Omega} V_{\text{ext}} \tilde{\phi}_{\ell,h}(x) \tilde{\phi}_{\ell,h}^*(x) dx \\
& + \sum_{s=1}^N \int_{\Omega} \int_{\Omega} \frac{|\phi_{s,Hh}(y)|^2}{|x-y|} dy \tilde{\phi}_{\ell,h}(x) \tilde{\phi}_{\ell,h}^*(x) dx \\
& + \sum_{s=1}^N \int_{\Omega} \int_{\Omega} \frac{\phi_{s,Hh}^*(y) \tilde{\phi}_{\ell,h}(y)}{|x-y|} dy \phi_{s,Hh}(x) \tilde{\phi}_{\ell,h}^*(x) dx.
\end{aligned} \tag{4.27}$$

Denote

$$\beta_{\text{Kin},\ell} = \frac{1}{2} \int_{\Omega} \nabla \tilde{\phi}_{\ell,h}(x) \nabla \tilde{\phi}_{\ell,h}^*(x) dx + \int_{\Omega} V_{\text{ext}} \tilde{\phi}_{\ell,h}(x) \tilde{\phi}_{\ell,h}^*(x) dx, \tag{4.28}$$

$$\beta_{\text{Har},s,\ell} = \int_{\Omega} \int_{\Omega} \frac{|\phi_{s,Hh}(y)|^2}{|x-y|} dy \tilde{\phi}_{\ell,h}(x) \tilde{\phi}_{\ell,h}^*(x) dx, \tag{4.29}$$

$$\beta_{\text{x},s,\ell} = \int_{\Omega} \int_{\Omega} \frac{\phi_{s,Hh}^*(y) \tilde{\phi}_{\ell,h}(y)}{|x-y|} dy \phi_{s,Hh}(x) \tilde{\phi}_{\ell,h}^*(x) dx. \tag{4.30}$$

It is obvious that $\beta_{\text{Kin},\ell}$ remains unchanged during the correction step. For $\beta_{\text{Har},s,\ell}$ and $\beta_{\text{x},s,\ell}$, when $s \neq \ell$, we have

$$\begin{aligned}
& \beta_{\text{Har},s,\ell} + \beta_{\text{x},s,\ell} \\
= & \int_{\Omega} \int_{\Omega} \frac{|\tilde{\phi}_{s,h}(y)|^2}{|x-y|} dy \tilde{\phi}_{\ell,h}(x) \tilde{\phi}_{\ell,h}^*(x) dx + \int_{\Omega} \int_{\Omega} \frac{\tilde{\phi}_{s,h}^*(y) \tilde{\phi}_{\ell,h}(y)}{|x-y|} dy \tilde{\phi}_{s,h}(x) \tilde{\phi}_{\ell,h}^*(x) dx \\
= & \int_{\Omega} \tilde{\tilde{V}}_{s,s}(x) \tilde{\phi}_{\ell,h}(x) \tilde{\phi}_{\ell,h}^*(x) dx + \int_{\Omega} \tilde{\tilde{V}}_{\ell,s}(x) \tilde{\phi}_{s,h}(x) \tilde{\phi}_{\ell,h}^*(x) dx
\end{aligned} \tag{4.31}$$

and

$$\begin{aligned}
& \beta_{\text{Har},\ell,\ell} + \beta_{\text{x},\ell,\ell} \\
= & \int_{\Omega} \int_{\Omega} \frac{|\tilde{\theta} \tilde{\phi}_{\ell,h}(y) + \sum_{m=1}^{N_H} c_{m,H} \psi_{m,H}(y)|^2}{|x-y|} dy \tilde{\phi}_{\ell,h}(x) \tilde{\phi}_{\ell,h}^*(x) dx \\
& + \int_{\Omega} \left\{ \int_{\Omega} \frac{(\tilde{\theta} \tilde{\phi}_{\ell,h}(y) + \sum_{m=1}^{N_H} c_{m,H} \psi_{m,H}(y))^* \tilde{\phi}_{\ell,h}(y)}{|x-y|} dy \right. \\
& \quad \left. \left(\tilde{\theta} \tilde{\phi}_{\ell,h}(x) + \sum_{m=1}^{N_H} c_{m,H} \psi_{m,H}(x) \right) \tilde{\phi}_{\ell,h}^*(x) \right\} dx \\
= & \int_{\Omega} \left\{ \left(|\tilde{\theta}|^2 \tilde{\tilde{V}}_{\ell,\ell}(x) + \tilde{\theta} \sum_{m=1}^{N_H} c_{m,H}^* \tilde{V}_{\ell,m}(x) + \tilde{\theta}^* \sum_{m=1}^{N_H} c_{m,H} \tilde{V}_{\ell,m}^*(x) + \sum_{m,n=1}^{N_H} c_{m,H} c_{n,H}^* V_{m,n}(x) \right) \right. \\
& \quad \left. \left(\tilde{\theta} \tilde{\phi}_{\ell,h}(x) + \sum_{m=1}^{N_H} c_{m,H} \psi_{m,H}(x) \right) \tilde{\phi}_{\ell,h}^*(x) \right\} dx
\end{aligned}$$

$$\begin{aligned}
& \tilde{\phi}_{\ell,h}(x) \tilde{\phi}_{\ell,h}^*(x) \Big\} dx \\
& + \int_{\Omega} \left(\tilde{\theta}^* \tilde{\tilde{V}}_{\ell,\ell}(x) + \sum_{m=1}^{N_H} c_{m,H}^* \tilde{V}_{\ell,m}(x) \right) \left(\tilde{\theta} \tilde{\phi}_{\ell,h}(x) + \sum_{m=1}^{N_H} c_{m,H} \psi_{m,H}(x) \right) \tilde{\phi}_{\ell,h}^*(x) dx. \tag{4.32}
\end{aligned}$$

Define

$$\tilde{\tilde{V}}_{s,m,j,\ell} = \int_{\Omega} \tilde{\tilde{V}}_{s,m}(x) \tilde{\phi}_{j,h}(x) \tilde{\phi}_{\ell,h}^*(x) dx. \tag{4.33}$$

It is obvious that $\tilde{\tilde{V}}_{s,m,j,\ell}$ remains unchanged during the correction step. Then β can be assembled in the following way

$$\beta_{\text{Har},s,\ell} + \beta_{x,s,\ell} = \tilde{\tilde{V}}_{s,s,\ell,\ell} + \tilde{\tilde{V}}_{\ell,s,s,\ell} \tag{4.34}$$

and

$$\begin{aligned}
& \beta_{\text{Har},\ell,\ell} + \beta_{x,\ell,\ell} \\
= & |\tilde{\theta}|^2 \tilde{\tilde{V}}_{\ell,\ell,\ell,\ell} + \tilde{\theta} \sum_{m=1}^{N_H} c_{m,H}^* \tilde{\tilde{V}}_{\ell,\ell,\ell,m} + \tilde{\theta}^* \sum_{m=1}^{N_H} c_{m,H} \tilde{\tilde{V}}_{\ell,\ell,\ell,m}^* + \sum_{m,n=1}^{N_H} c_{m,H} c_{n,H}^* \tilde{\tilde{V}}_{\ell,m,n} \\
& + |\tilde{\theta}|^2 \tilde{\tilde{V}}_{\ell,\ell,\ell,\ell} + \tilde{\theta}^* \sum_{m=1}^{N_H} c_{m,H} \tilde{\tilde{V}}_{\ell,\ell,\ell,m}^* + \tilde{\theta} \sum_{m=1}^{N_H} c_{m,H}^* \tilde{\tilde{V}}_{\ell,\ell,\ell,m} + \sum_{m,n=1}^{N_H} c_{m,H} c_{n,H}^* \tilde{\tilde{W}}_{*,\ell,m,n}. \tag{4.35}
\end{aligned}$$

As we can see, to construct the stiffness matrix in (4.1), we just need to compute:

1. Two tensors \mathbf{V} and $\tilde{\mathbf{V}}_{\ell}$ with $(\mathbf{V})_{m,n,i,j} = V_{m,n,i,j}$ and $(\tilde{\mathbf{V}}_{\ell})_{m,i,j} = \tilde{V}_{\ell,m,i,j}$.
2. Three matrices $\tilde{\tilde{\mathbf{V}}}_{\ell}$, $\tilde{\mathbf{W}}_{\ell}$, $\tilde{\mathbf{W}}_{*,\ell}$ with $(\tilde{\tilde{\mathbf{V}}}_{\ell})_{i,j} = \tilde{\tilde{V}}_{\ell,i,j}$, $(\tilde{\mathbf{W}}_{\ell})_{i,j} = \tilde{W}_{\ell,i,j}$, $(\tilde{\mathbf{W}}_{*,\ell})_{i,j} = \tilde{W}_{*,\ell,i,j}$.
3. One vector $\tilde{\tilde{\mathbf{V}}}_{\ell}$ with $(\tilde{\tilde{\mathbf{V}}}_{\ell})_i = \tilde{\tilde{V}}_{\ell,\ell,\ell,i}$.
4. One scalar $\tilde{\tilde{V}}_{\ell}$ with $\tilde{\tilde{V}}_{\ell} = \tilde{V}_{\ell,\ell,\ell,\ell}$.

Besides, we need to compute some matrices and vectors that depend on the other wavefunctions:

5. Two matrices $\tilde{\tilde{\mathbf{V}}}_{1\ell}$, $\tilde{\tilde{\mathbf{V}}}_{2\ell}$ with $(\tilde{\tilde{\mathbf{V}}}_{1\ell})_{s,i} = \tilde{\tilde{V}}_{s,s,\ell,i}$, $(\tilde{\tilde{\mathbf{V}}}_{2\ell})_{s,i} = \tilde{\tilde{V}}_{\ell,s,s,i}$.
6. Two vectors $\tilde{\tilde{\mathbf{V}}}_{1\ell}$ and $\tilde{\tilde{\mathbf{V}}}_{2\ell}$ with $(\tilde{\tilde{\mathbf{V}}}_{1\ell})_s = \tilde{V}_{s,s,\ell,\ell}$ and $(\tilde{\tilde{\mathbf{V}}}_{2\ell})_s = \tilde{V}_{\ell,s,s,\ell}$.

For these quantities, the tensor \mathbf{V} remains unchanged throughout the algorithm, thus \mathbf{V} only needs to be computed one time at the beginning of the algorithm. The other quantities remain unchanged in the SCF iteration of each correction space, thus these quantities only need to be computed one time before the SCF iteration in each correction space.

Based on the definitions of these quantities, the main point is to compute the involved functions $\tilde{V}_{\ell,s}(x)$, $\tilde{V}_{\ell,m}(x)$ and $V_{m,n}(x)$.

To compute the functions $\tilde{V}_{\ell,s}(x)$, $\tilde{V}_{\ell,m}(x)$ and $V_{m,n}(x)$, we need to solve some Poisson equations as follows:

$$-\Delta \tilde{V}_{\ell,s}(x) = 4\pi \tilde{\phi}_{\ell,h} \tilde{\phi}_{s,h}^*, \quad s = 1, \dots, N, \tag{4.36}$$

$$-\Delta \tilde{V}_{\ell,m}(x) = 4\pi \tilde{\phi}_{\ell,h} \psi_{m,H}, \quad m = 1, \dots, N_H, \tag{4.37}$$

$$-\Delta V_{m,n}(x) = 4\pi\psi_{m,H}\psi_{n,H}, \quad m, n = 1, \dots, N_H. \quad (4.38)$$

Because the coarse space V_H is fixed, the equations (4.38) only need to be solved one time for the entire algorithm. These functions can even be stored in the package in advance. The equations (4.36) and (4.37) only need to be solved before the SCF iteration in each correction space.

Remark 4.1. *In the multilevel correction type of AFEM, we need to solve some linearized boundary value problems in adaptive finite element spaces. For these boundary value problems, the exchange potentials are linearized by the approximate wavefunctions derived from the previous mesh level. Then we will obtain a sparse system of equations that can be solved efficiently. Next, we will briefly describe how to assemble the vector corresponding to the exchange potential. In fact, after deriving the approximate wavefunctions based on the above mentioned process, we can assemble $V_x(P_{h_{k+1}})$ on $V_{H,h_{k+1}}$ first, and then prolong the exchange potential from $V_{H,h_{k+1}}$ to $V_{h_{k+2}}$. This will form the righthand side term of the linearized boundary value problem defined in $V_{h_{k+2}}$.*

Assume the final approximate solution derived in $V_{H,h_{k+1}}$ is denoted by

$$\phi_{\ell,Hh} = \tilde{\theta}_\ell \tilde{\phi}_{\ell,h} + \sum_{m=1}^{N_H} c_{m,H,\ell} \psi_{m,H}.$$

To discretize the exchange potential, the key point is to derive $\int_{\Omega} \frac{\phi_{\ell,Hh}(y) \phi_{s,Hh}(y)}{|x-y|} dy$. By simple calculations, we can derive

$$\begin{aligned} & \int_{\Omega} \frac{\phi_{\ell,Hh}(y) \phi_{s,Hh}^*(y)}{|x-y|} dy \\ &= \int_{\Omega} \frac{(\tilde{\theta}_\ell \tilde{\phi}_{\ell,h}(y) + \sum_{m=1}^{N_H} c_{m,H,\ell} \psi_{m,H}(y)) (\tilde{\theta}_s^* \tilde{\phi}_{s,h}^*(y) + \sum_{m=1}^{N_H} c_{m,H,s}^* \psi_{m,H}(y))}{|x-y|} dy \\ &= \tilde{\theta}_\ell \tilde{\theta}_s^* \tilde{\tilde{V}}_{\ell,s} + \sum_{m=1}^{N_H} c_{m,H,\ell} \tilde{\theta}_s^* \tilde{V}_{s,m}^* + \sum_{m=1}^{N_H} c_{m,H,s}^* \tilde{\theta}_\ell \tilde{V}_{\ell,m} + \sum_{m,n=1}^{N_H} c_{m,H,\ell} c_{n,H,s}^* V_{m,n}. \end{aligned}$$

We can see that all the required components have already been derived when we solve the small-scale Hartree-Fock equation in the correction space. Thus, only a few matrix and tensor operations are required to discretize the exchange potential.

In Algorithm 4.1, based on above discussion and preparation, we propose the efficient implementation strategy for Algorithm 3.3.

Algorithm 4.1. *Efficient implementation strategy for Algorithm 3.3*

1. Compute the matrices M_H as (4.2), A_{Kin} as (4.4), compute $V_{m,n}$ according to (4.38) and then compute the tensor \mathbf{V} as (4.11) in the coarse space V_H .
2. Solve the Hartree-Fock equation (3.7) in the initial finite element space V_{h_1} .
3. Set $k = 1$.
4. Compute the local error indicators $\eta_{h_k}(\{\lambda_{\ell,h_k}, \phi_{\ell,h_k}\}_{\ell=1}^N, T)$ for each element $T \in \mathcal{T}_{h_k}$.
5. Construct $\mathcal{M}_{h_k} \subset \mathcal{T}_{h_k}$ by Dörfler's marking strategy and refine \mathcal{T}_{h_k} to get a new mesh $\mathcal{T}_{h_{k+1}}$.
6. Solve the linear boundary value problem (3.1) to derive $\tilde{\phi}_{\ell,h_{k+1}} \in V_{h_{k+1}}$, $\ell = 1, \dots, N$.
7. For $\ell = 1, \dots, N$:
 - (A) Define $V_{H,h_{k+1}} = V_H + \text{span}\{\tilde{\phi}_{\ell,h_{k+1}}\}$ and compute the following quantities:
 - (1) Compute $\tilde{\tilde{V}}_{\ell,s}(x)$, $s = 1, \dots, N$ and $\tilde{V}_{\ell,m}(x)$, $m = 1, \dots, N_H$ as (4.36) and (4.37).
 - (2) Compute the tensor $\tilde{\mathbf{V}}_\ell$ as (4.12), three matrices $\tilde{\tilde{\mathbf{V}}}_\ell$, $\tilde{\mathbf{W}}_\ell$, $\tilde{\mathbf{W}}_{*,\ell}$ as (4.13) (4.14) and (4.15), a vector $\tilde{\tilde{\mathbf{V}}}_\ell$ as (4.24) and a scalar $\tilde{\tilde{V}}_\ell$ as (4.33).

(3) Compute two matrices $\tilde{\tilde{\mathbf{V}}}_{1\ell}$, $\tilde{\tilde{\mathbf{V}}}_{2\ell}$ as (4.24), two vectors $\tilde{\tilde{\mathbf{V}}}_{1\ell}$ and $\tilde{\tilde{\mathbf{V}}}_{2\ell}$ as (4.33).
 (4) Compute the vector b_{Kin} as (4.19) and the scalar β_{Kin} as (4.28).
 (5) Compute the vector c_{Hh} and the scalar γ as (4.2).

(B) Do the following loop:

- (1) Compute $A_{\text{Har},s} + A_{x,s}$ as (4.16) and (4.17). Then $A_H = A_{\text{Kin}} + \sum_s (A_{\text{Har},s} + A_{x,s})$.
- (2) Compute $b_{\text{Har},s,\ell} + b_{x,s,\ell}$ as (4.25) and (4.26). Then $b_{Hh} = b_{\text{Kin}} + \sum_s (b_{\text{Har},s,\ell} + b_{x,s,\ell})$.
- (3) Compute $\beta_{\text{Har},s,\ell} + \beta_{x,s,\ell}$ as (4.34) and (4.35). Then $\beta = \beta_{\text{Kin}} + \sum_s (\beta_{\text{Har},s,\ell} + \beta_{x,s,\ell})$.
- (4) Solve the eigenvalue problem (4.1).
- (5) If the desired accuracy is satisfied, stop. Else, go to step (1) of (B) and continue.

8. Let $k = k + 1$ and go to step 4.

Remark 4.2. As we can see, during the SCF iteration in the 7(B) step of Algoirthm 4.1, we just need to perform some small-scale matrix and tensor calculations. No additional matrix assembling are needed. Thus, the correction step can be implemented efficiently.

Next, we briefly analyze the computational work for solving the ℓ -th wavefunction. Assume that the linearized boundary value problems can be solved with linear computational work based on some efficient numerical methods such as the multigrid method. Then for the boundary value problem (3.1), the computational work is $O(N_k)$.

For the boundary value problems (4.36), the computational work is $O(NN_k)$.

For the boundary value problems (4.37), the computational work is $O(N_H N_k)$.

For the tensor $\tilde{\mathbf{V}}_\ell$ as (4.12), the computational work is $O(N_H N_k)$.

For the matrix $\tilde{\mathbf{V}}_\ell$ as (4.13), the computational work is $O(N_k)$.

For the matrices $\tilde{\mathbf{W}}_\ell$, $\tilde{\mathbf{W}}_{*,\ell}$ as (4.14) and (4.15), the computational work is $O(N_H N_k)$.

For the vector $\tilde{\mathbf{V}}_\ell$ as (4.24) and a scalar \tilde{V}_ℓ as (4.33), the computational work is $O(N_k)$.

For the two matrices $\tilde{\tilde{\mathbf{V}}}_{1\ell}$, $\tilde{\tilde{\mathbf{V}}}_{2\ell}$ as (4.24), the computational work is $O(NN_k)$.

For the two vectors $\tilde{\tilde{\mathbf{V}}}_{1\ell}$ and $\tilde{\tilde{\mathbf{V}}}_{2\ell}$ as (4.33), the computational work is $O(NN_k)$.

For the vector b_{Kin} as (4.19) and the scalar β_{Kin} as (4.28), the computational work is $O(N_k)$.

For the vector c_{Hh} and the scalar γ as (4.2), the computational work is $O(N_k)$.

During the SCF iteration, we need to perform some matrix operations:

For $A_H = A_{\text{Kin}} + \sum_s (A_{\text{Har},s} + A_{x,s})$, the computational work is $O(NN_H^2 + N_H^3)$.

For $b_{Hh} = b_{\text{Kin}} + \sum_s (b_{\text{Har},s,\ell} + b_{x,s,\ell})$, the computational work is $O(NN_H + N_H^3)$.

For $\beta = \beta_{\text{Kin}} + \sum_s (\beta_{\text{Har},s,\ell} + \beta_{x,s,\ell})$, the computational work is $O(N + N_H^2)$.

Assume ω times SCF iteration are needed and the computational work for small-scale linear eigenvalue problem (4.1) is $O(M_H)$. Then the total computational work is

$$O((N + N_H)N_k + \omega(NN_H^2 + N_H^3 + M_H)). \quad (4.39)$$

For a given molecular system, to derive a more accurate approximation, the value of N_k is going to get increasingly larger. However, the number of electrons and the dimension of correction space remain fixed. In other words, the values of N , N_H and M_H remain unchanged. In addition, the coefficient of N_k in (4.39) is independent from the iteration time ω . Thus, a linear computational work can be obtained with the refinement of mesh, which is gradually freed from the influence of the number of SCF iterations.

Remark 4.3. In terms of storage, direct AFEM needs to store large-scale dense matrices which involves $O(N_k^2)$ data. In the proposed algorithm, the involved dense matrices are $\tilde{\mathbf{W}}_\ell$, $\tilde{\mathbf{W}}_{*,\ell}$, $\tilde{\tilde{\mathbf{V}}}_{1\ell}$, $\tilde{\tilde{\mathbf{V}}}_{2\ell}$. The dimension $\dim(\tilde{\mathbf{W}}_\ell) = \dim(\tilde{\mathbf{W}}_{*,\ell}) = N_H \times N_H$, $\dim(\tilde{\tilde{\mathbf{V}}}_{1\ell}) = \dim(\tilde{\tilde{\mathbf{V}}}_{2\ell}) = N \times N_H$. Thus, the amount of data to be stored are $O(NN_H + N_H^2)$. The total number of stored data are $O(N_k + NN_H + N_H^2)$, which is a significant improvement over the direct AFEM.

Remark 4.4. Finally, we highlight that Algorithm 4.1 is inherently suitable for eigenpairwise parallel computing due to its distinctive structure. Notably, Algorithm 4.1 handles different orbits independently, thus circumventing the need for large-scale inner product computation for orthogonalization, which often poses a bottleneck in parallel computing. Consequently, this strategy facilitates parallel computing by allowing different wavefunctions to be processed concurrently on separate processors.

5 Numerical experiments

In this section, we present several numerical examples to validate the efficiency of the proposed numerical method. These numerical examples are performed on a cluster with 90 nodes. Each computing node has two 20-core with Intel Xeon E5-2660 v3 processors at 2.6 GHz and 192 GB memory.

In our numerical experiments, we consider the Hartree–Fock equation for Lithium (HLi), Methane (CH_4), Benzene(C_6H_6) and Ethanol($\text{C}_2\text{H}_6\text{O}$). To exhibit the advantages of the proposed algorithm, we compare the numerical results with the direct adaptive finite element method (i.e. solving Hartree–Fock equation by Algorithm 2.1 directly in each adaptive finite element space) from four perspectives including precision, solving efficiency, memory consumption and parallel scalability. For both Algorithm 4.1 and direct AFEM, the linear finite element basis are employed.

5.1 Precision

In this subsection, we aim to exhibit the accuracy of Algorithm 4.1. For this end, we present the approximate energies derived from Algorithm 4.1 and the results based on Gaussian basis functions employing the computational chemistry package NWChem [59] in Table 1.

From Table 1, we can find that Algorithm 4.1 is able to derive quite accurate approximate solutions as that of NWChem.

Atom	Energy of Algorithm 4.1	Energy of NWChem
Lithium hydride	-7.9842	-7.9842
Methane	-40.1998	-40.1996
Ethanol	-154.1057	-154.1065
Benzene	-230.7265	-230.7284

Table 1: The approximate energies derived by Algorithm 4.1 and NWChem.

5.2 Solving efficiency

In this subsection, we present the computational time (in seconds) of Algorithm 4.1 and direct AFEM with the refinement of mesh. The corresponding results and the acceleration ratio between the two algorithms are presented in Tables 2–5. The acceleration ratio is obtained by dividing the time of direct AFEM by the time of Algorithm 4.1. The symbol “–” means the computer runs out of memory. From Tables 2–5, we can find that Algorithm 4.1 has a significant advantage over the direct AFEM. First, for the same molecule, we can see that the advantage increases with the refinement of mesh. Next, for different molecules, we can see that the advantage becomes more apparent for more complex models.

Atom	Time of direct AFEM	Time of Algorithm 4.1	Ratio
Lithium hydride	1.4466E+5	1.6407E+2	8.8171E+2
Methane	5.3731E+5	3.0857E+2	1.7412E+3
Ethanol	-	1.1323E+3	-
Benzene	-	2.4201E+3	-

Table 2: The computational time (in seconds) of the direct AFEM, Algorithm 4.1 with the same energy accuracy 1E-1 and the acceleration ratio.

Atom	Time of direct AFEM	Time of Algorithm 4.1	Ratio
Lithium hydride	2.7947E+6	3.0526E+2	9.1551E+3
Methane	1.0986E+7	5.8011E+2	1.8939E+4
Ethanol	-	2.1288E+3	-
Benzene	-	4.5493E+3	-

Table 3: The computational time (in seconds) of the direct AFEM, Algorithm 4.1 with the same energy accuracy 1E-2 and the acceleration ratio.

Atom	Time of direct AFEM	Time of Algorithm 4.1	Ratio
Lithium hydride	-	1.1323E+3	-
Methane	-	2.2079E+3	-
Ethanol	-	7.8043E+3	-
Benzene	-	1.6623E+4	-

Table 4: The computational time (in seconds) of the direct AFEM, Algorithm 4.1 with the same energy accuracy 1E-3 and the acceleration ratio.

5.3 Memory consumption

A major challenge in solving the Hartree–Fock equation is that traditional algorithms generate dense matrices, which consume a large amount of memory. Our algorithm, however, avoids generating large-scale dense matrices, resulting in significant memory savings. This result is verified by the numerical data presented in Tables 6–9, which show that the memory requirement of our algorithm is greatly reduced compared to that of the direct AFEM. Meanwhile, the memory usage analysis reveals that the algorithm’s advantages become increasingly prominent when handling larger-scale computations and more complex models.

5.4 Parallel scalability

In the last subsection, we evaluate the parallel scalability of Algorithm 4.1. We calculate the trend of the parallel efficiency of Algorithm 4.1 with the increase of the computing scale. The corresponding results are presented in Figure 1, which shows that quite a good parallel scalability can be obtained through solving different wavefunctions by different computing nodes.

6 Conclusion

This paper presented an efficient multilevel correction type of adaptive algorithm for Hartree–Fock equation, significantly improving computational efficiency while maintaining accuracy. The method transforms the Hartree–Fock equation into tractable linearized boundary value problems and small-scale Hartree–Fock equations in low-dimensional correction spaces, avoiding direct computation of large-scale nonlinear eigenvalue problems and dense matrices. Other key points include independent construction of correction spaces for parallelization, tensor-based preprocessing for computational reuse. This approach enables efficient three-dimensional Hartree–Fock calculations and provides a solid foundation for accurate electronic structure simulations of complex systems.

Atom	Time of direct AFEM	Time of Algorithm 4.1	Ratio
Lithium hydride	-	2.4202E+3	-
Methane	-	4.5560E+3	-
Ethanol	-	1.6765E+4	-
Benzene	-	3.5623E+4	-

Table 5: The computational time (in seconds) of the direct AFEM, Algorithm 4.1 with the same energy accuracy 1E-4 and the acceleration ratio.

Atom	Memory of direct AFEM	Memory of Algorithm 4.1	Ratio
Lithium hydride	1.1601E+1	1.0767E-1	1.0774E+2
Methane	7.6577E+1	1.4260E-1	5.3697E+2
Ethanol	-	1.5974E-1	-
Benzene	-	2.3050E-1	-

Table 6: The memory (in GB) of the direct AFEM, Algorithm 4.1 with the same energy accuracy 1E-1 and the consumption ratio.

Atom	Memory of direct AFEM	Memory of Algorithm 4.1	Ratio
Lithium hydride	2.3001E+1	1.4887E-1	1.5450E+2
Methane	1.8694E+2	1.7475E-1	1.0697E+3
Ethanol	-	2.1387E-1	-
Benzene	-	2.4281E-1	-

Table 7: The memory (in GB) of the direct AFEM, Algorithm 4.1 with the same energy accuracy 1E-2 and the consumption ratio.

Atom	Memory of direct AFEM	Memory of Algorithm 4.1	Ratio
Lithium hydride	-	2.6732E-1	-
Methane	-	3.2284E-1	-
Ethanol	-	4.0338E-1	-
Benzene	-	5.6582E-1	-

Table 8: The memory (in GB) of the direct AFEM, Algorithm 4.1 with the same energy accuracy 1E-3 and the consumption ratio.

Atom	Memory of direct AFEM	Memory of Algorithm 4.1	Ratio
Lithium hydride	-	8.9169E-1	-
Methane	-	1.1426E+1	-
Ethanol	-	1.3787E+1	-
Benzene	-	2.0454E+1	-

Table 9: The memory (in GB) of the direct AFEM, Algorithm 4.1 with the same energy accuracy 1E-4 and the consumption ratio.

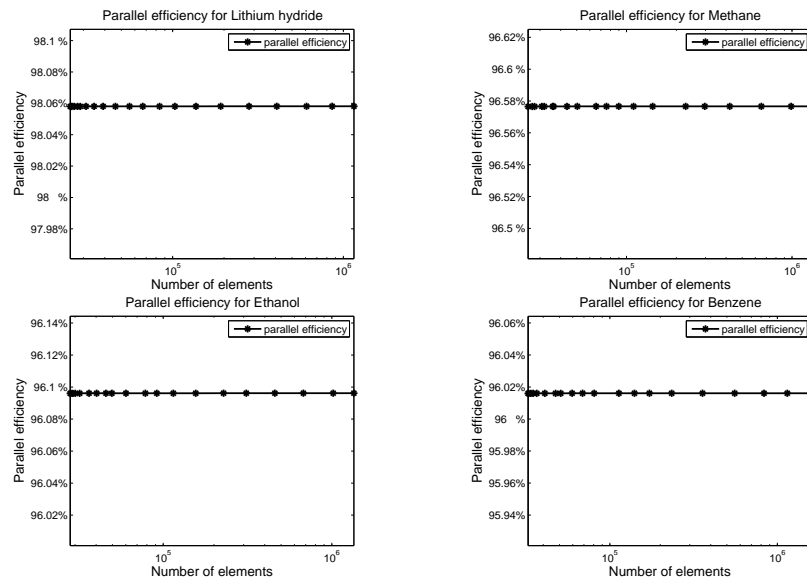


Figure 1: Parallel efficiency of Algorithm 4.1 for Lithium, Methane, Benzene and Ethanol.

References

- [1] R. A. Adams, *Sobolev spaces*, Academic Press, New York, 1975.
- [2] J. Ackermann, B. Erdmann and R. Roitzsch, *A self-adaptive multilevel finite element method for the stationary Schrödinger equation in three space dimensions*, J. Chem. Phys., 101 (1994), 7643–7650.
- [3] J. Ackermann and R. Roitzsch, *A two-dimensional multilevel adaptive finite element method for the time-independent Schrödinger equation*, Chem. Phys. Lett., 214 (1993), 109–117.
- [4] R. Alizadegan, K. J. Hsia and T. J. Martinez, *A divide and conquer real space finite-element Hartree–Fock method*, J. Chem. Phys., 132 (2010), 034101.
- [5] D. G. Anderson, *Iterative procedures for nonlinear integral equations*, J. Assoc. Comput. Mach., 12(4) (1965), 547–560.
- [6] I. Babuška and W.C. Rheinboldt, *Error estimates for adaptive finite element computations*, SIAM J. Numer. Anal., 15 (1978), 736–754.
- [7] G. Bao, G. Hu and D. Liu, *Numerical solution of the Kohn-Sham equation by finite element methods with an adaptive mesh redistribution technique*, J. Sci. Comput., 55(2) (2012), 372–391.
- [8] A. D. Becke, *A new mixing of Hartree–Fock and local density-functional theories*, J. Chem. Phys., 98 (1993), 1372–1377.
- [9] N. M Boffi, M. Jain and A. Natan, *Efficient computation of the Hartree–Fock exchange in real-space with projection operators*, J. Chem. Theory Comput., 12(8) (2016), 3614–3622.
- [10] M. Braun, *Finite element Hartree–Fock calculations in three dimensions for atoms and small molecules*, J. Comput. Appl. Math., 270 (2014), 100–108.
- [11] M. Braun and K. O. Obodo, *Finite element density functional calculations for light molecules using a cusp factor to mitigate the Coulomb potential*, Eur. Phys. J. B, 92 (2019), 230.
- [12] O. Beck, D. Heinemann and D. Kolb, *Fast and accurate molecular Hartree–Fock with a finite-element multigrid method*, 2003, arXiv:physics/0307108.
- [13] H. Bethe and R. Jackiw, *Intermediate quantum mechanics*, New York, Benjamin, 1969.
- [14] J. M. Cascon, C. Kreuzer, R. H. Nochetto and K. G. Siebert, *Quasi-optimal convergence rate for an adaptive finite element method*, SIAM J. Numer. Anal., 46(5) (2008), 2524–2550.
- [15] W. Dörfler, *A convergent adaptive algorithm for Poisson’s equation*, SIAM J. Numer. Anal., 33(3) (1996), 1106–1124.
- [16] I. Duchemin and F. Gygi, *A scalable and accurate algorithm for the computation of Hartree–Fock exchange*, Comput. Phys. Commun., 181 (2010), 855–860.
- [17] O. T. Filho, J. C. Pinheiro and R. T. Kondo, *The generator coordinate Hartree–Fock method as strategy for building Gaussian basis sets to ab initio study of the process of adsorption of sulfur on platinum (200) surface*, J. Mol. Struct. (Theochem), 716 (2005), 89–92.
- [18] J. R. Flores, E. Clementi and V. Sonnad, *Solution of atomic Hartree–Fock equations with the P version of the finite element method*, J. Chem. Phys., 91 (1989), 7030.
- [19] J. R. Flores, E. Clementi and V. Sonnad, *A p-version finite-element approach for atomic Hartree–Fock calculations*, Chem. Phys. Lett., 163 (1989), 198–201.
- [20] V. Fock, *Näherungsmethode zur Lösung des quantenmechanischen Mehrkörperproblems*, Z. Physik, 61 (1930), 126–148.
- [21] P. Giannozzi et al., *QUANTUM ESPRESSO: a modular and open-source software project for quantum simulations of materials*, J. Phys.: Condens. Matter, 21 (2009), 395502.

[22] I. I. Guseinov, B. A. Mamedov and R. Aydin, *Computation of molecular integrals over Slater-type orbitals. IV. Calculation of multicenter electron-repulsion integrals using recurrence relations for overlap integrals*, J. Mol. Struct. (Theochem), 503 (2000), 179–188.

[23] I. I. Guseinov et al, *Computation of overlap integrals over Slater-type orbitals using auxiliary functions*, Int. J. Quantum Chem., 67 (1998), 199–204.

[24] D. Hartree, *The calculation of atomic structures*, New York, Wiley, 1957.

[25] D. Heinemann, B. Fricke and D. Kolb, *Solution of the Hartree–Fock–Slater equations for diatomic molecules by the finite-element method*, Phys. Rev. A, 38 (1988), 4994–5001.

[26] D. Heinemann, A. Rosen and B. Fricke, *Spin-polarized Hartree–Fock–Slater calculations in atoms and diatomic molecules with the finite element method*, Chem. Phys. Lett., 166 (1990), 627–629.

[27] J. Heyd, G. Scuseria and M. Ernzerhof, *Hybrid functionals based on a screened Coulomb potential*, J. Chem. Phys., 118(18) (2003), 8207–8215.

[28] P. Hohenberg and W. Kohn, *Inhomogeneous electron gas*, Phys. Rev., 136 (1964), B864–B871.

[29] Q. Hong , H. Xie and F. Xu, *A multilevel correction type of adaptive finite element method for eigenvalue problems*, SIAM J. Sci. Comput., 40(6) (2018), A4208–A4235.

[30] G. Hu, H. Xie and F. Xu, *On accelerating a multilevel correction adaptive finite element method for Kohn-Sham equation*, J. Comput. Phys., 472 (2023), 111674.

[31] W. Hu, L. Lin, A. S. Banerjee, E. Vecharynski and C. Yang, *Adaptively compressed exchange operator for large-scale hybrid density functional calculations with applications to the adsorption of water on Silicene*, J. Chem. Theory Comput., 13(3) (2017), 1188–1198.

[32] W. Hu, L. Lin and C. Yang, *Projected commutator DIIS method for accelerating hybrid functional electronic structure calculations*, J. Chem. Theory Comput., 13 (2017), 5458–5467.

[33] W. Kohn and L. Sham, *Self-consistent equations including exchange and correlation effects*, Phys. Rev. A, 140 (1965), 1133–1138.

[34] G. Kresse and G. J. Furthmüller, *Efficient iterative schemes for ab initio total-energy calculations using a plane-wave basis set*, Phys. Rev. B, 5 (1996), 11169–11186.

[35] C. Lavor, L. Liberti, N. Maculan and M. A. C. Nascimento, *Solving Hartree–Fock systems with global optimization methods*, Europhys. Lett., 77 (2007), 50006.

[36] S. Lehtola, *Fully numerical Hartree–Fock and density functional calculations. II. Diatomic molecules*, Int. J. Quantum Chem., 119 (2019), e25944.

[37] S. Lehtola, *Fully numerical Hartree–Fock and density functional calculations. I. Atoms*, Int. J. Quantum Chem., 119 (2019), e25945.

[38] S. Lehtola, *A review on non-relativistic, fully numerical electronic structure calculations on atoms and diatomic molecules*, Int. J. Quantum Chem., 119 (2019), e25968.

[39] S. Lehtola, *HelFEM-Finite element methods for electronic structure calculations on small systems*, <http://github.com/susilehtola/HelFEM>, 2024.

[40] E. H. Lieb and B. Simon, *The Hartree–Fock theory for Coulomb systems*, Commun. Math. Phys., 53 (1977), 185–194.

[41] L. Lin, *Adaptively compressed exchange operator*, J. Chem. Theory Comput., 12 (2016), 2242–2249.

[42] Q. Lin and H. Xie, *A multi-level correction scheme for eigenvalue problems*, Math. Comp., 84(291) (2015), 71–88.

[43] P. L. Lions, *Solutions of Hartree–Fock equations for Coulomb systems*, Commun. Math. Phys., 109 (1987), 33–97.

[44] J. Lu and L. Ying, *Compression of the electron repulsion integral tensor intensor hypercontraction format with cubic scaling cost*, J. Comput. Phys., 302 (2015), 329–335.

[45] R. S. Mulliken, C. A. Rieke, D. Orloff, and H. Orloff, *Formulas and numerical tables for overlap integrals*, J. Chem. Phys., 17 (1949), 1248–1267.

[46] J. E. Pask, B. M. Klein, C. Y. Fong and P. A. Sterne, *Real-space local polynomial basis for solid-state electronic-structure calculations: A finite-element approach*, Phys. Rev. B, 59(190) (1999), 12352–12358.

[47] P. Pulay, *Improved SCF convergence acceleration*, J. Comput. Chem., 3 (1982), 556–560.

[48] J. P. Perdew and Y. Wang, *Accurate and simple density functional for the electronic exchange energy: Generalized gradient approximation*, Phys. Rev. B, 33 (1986), 8800–8802.

[49] H. M. Quiney, V. N. Glushkov and S. Wilson, *The Dirac equation in the algebraic approximation: VIII. Comparison of finite basis set and finite element molecular Dirac–Hartree–Fock calculations for the H₂, LiH, and BH ground states*, Int. J. Quantum Chem., 89 (2002), 227–236.

[50] M. Reeken, *General theorem on bifurcation and its application to the Hartree equation of the Helium atom*, J. Math. Phys., 11 (1970), 2505–2512.

[51] R. M. L. Savedra, J. C. Pinheiro, O. T. Filho and R. T. Kondo, *Gaussian basis sets by generator coordinate Hartree–Fock method to ab initio calculations of electron affinities of enolates*, J. Mol. Struct. (Theochem), 587 (2002), 9–17.

[52] H. F. Schaefer, *The Electronic Structure of Atoms and Molecules. A survey of rigorous quantum mechanical results*, Addison-Wesley Pub Co, 1972.

[53] M. D. Segall, *First-principles simulation: ideas, illustrations and the CASTEP code*, J. Phys.: Condens. Matter, 14 (2002), 2717–2744.

[54] J. H. Skone, M. Govoni and G. Galli, *Self-consistent hybrid functional for condensed systems*, Phys. Rev. B, 89 (2014), 195112.

[55] J. C. Slater, *Note on Hartree’s Method*, Phys. Rev., 35 (1930), 210–211.

[56] J.C. Slater, *Quantum theory of atomic structure*, Vol. I. NewYork, McGraw-Hill, 1960.

[57] D. Sundholm and J. Olsen, *Finite-element multiconfiguration Hartree–Fock calculations of electron affinities of manganese*, Chem. Phys. Lett., 233 (1995), 115–122.

[58] D. Sundholm, J. Olsen and S. A. Alexander, *Finite-element multiconfiguration Hartree–Fock calculations on the excitation energies and the ionization potential of oxygen*, J. Chem. Phys., 96 (1992), 5229–5232.

[59] M. Valiev, et al., *NWChem: a comprehensive and scalable open-source solution for large scale molecular simulations*, Comput. Phys. Commun., 181 (2010) 1477–1489.

[60] S. R. White, J. W. Wilkins and M. Teter, *Finite-element method for electronic structure*, Phys. Rev. B, 39 (1989), 5819–5833.

[61] D. B. Williams-Young, et al, *Distributed memory, GPU accelerated Fock construction for hybrid, Gaussian basis density functional theory*, J. Chem. Phys., 158 (2023), 234104.

[62] F. Xu, H. Xie and N. Zhang, *A parallel augmented subspace method for eigenvalue problems*, SIAM J. Sci. Comput., 42(5) (2020), A2655–A2677.

[63] T. D. Young, R. Vargas and J. Garza, *A Hartree–Fock study of the confined helium atom: Local and global basis set approaches*, Phys. Lett. A, 380 (2016), 712–717.

[64] W. Zheng and L. Ying, *Finite-element calculations for the Helium atom*, Int. J. Quantum Chem., 97 (2004), 659–669.